Gas-particle partitioning of primary organic aerosol emissions: 3. Biomass burning

Andrew A. May,[1,2] Ezra J. T. Levin,[2] Christopher J. Hennigan,[1,3] Ilona Riipinen,[1,4] Taehyoung Lee,[2,5] Jeffrey L. Collett Jr.,[2] Jose L. Jimenez,[6,7] Sonia M. Kreidenweis,[2] and Allen L. Robinson[1]

[1] Atmospheric organic aerosol concentrations depend in part on the gas-particle partitioning of primary organic aerosol (POA) emissions. Consequently, heating and dilution were used to investigate the volatility of biomass-burning smoke particles from combustion of common North American trees/shrubs/grasses during the third Fire Lab at Missoula Experiment. Fifty to eighty percent of the mass of biomass-burning POA evaporated when isothermally diluted from plume (~1000 $\mu g\, m^{-3}$) to ambient-like concentrations (~10 $\mu g\, m^{-3}$), while roughly 80% of the POA evaporated upon heating to 100°C in a thermodenuder with a residence time of ~14 sec. Therefore, the majority of the POA emissions were semivolatile. Thermodenuder measurements performed at three different residence times indicated that there were not substantial mass transfer limitations to evaporation (i.e., the mass accommodation coefficient appears to be between 0.1 and 1). An evaporation kinetics model was used to derive volatility distributions and enthalpies of vaporization from the thermodenuder data. A single-volatility distribution can be used to represent the measured gas-particle partitioning from the entire set of experiments, including different fuels, organic aerosol concentrations, and thermodenuder residence times. This distribution, derived from the thermodenuder measurements, also predicts the dilution-driven changes in gas-particle partitioning. This volatility distribution and associated emission factors for each fuel studied can be used to update emission inventories and to simulate the gas-particle partitioning of biomass-burning POA emissions in chemical transport models.

Additional supporting information may be found in the online version of this article.

[1]Center for Atmospheric Particle Studies, Carnegie Mellon University, Pittsburgh, Pennsylvania, USA.

[2]Department of Atmospheric Science, Colorado State University, Fort Collins, Colorado, USA.

[3]Department of Chemical, Biochemical, and Environmental Engineering, University of Maryland, Baltimore County, Baltimore, Maryland, USA.

[4]Department of Applied Environmental Science, Stockholm University, Stockholm, Sweden.

[5]Department of Environmental Science, Hankuk University of Foreign Studies, Seoul, South Korea.

[6]Department of Chemistry & Biochemistry, University of Colorado, Boulder, Colorado, USA.

[7]Cooperative Institute for Research in the Environmental Sciences, Boulder, Colorado, USA.

[8]Department of Mechanical Engineering, Carnegie Mellon University, Pittsburgh, Pennsylvania, USA.

Corresponding author: A. L. Robinson, Department of Mechanical Engineering, Carnegie Mellon University, 5000 Forbes Avenue, Pittsburgh, PA 15213, USA. (alr@andrew.cmu.edu)

1. Introduction

[2] Biomass-burning emissions contribute ~75% of global combustion primary organic aerosol (POA) [*Bond et al.*, 2004]. Until recently, POA has been assumed to be nonvolatile in emissions inventories and chemical transport models, but studies during the last decade have demonstrated that a large fraction of biomass-burning POA emissions is semivolatile [*Lipsky and Robinson*, 2006; *Grieshop et al.*, 2009; *Huffman et al.*, 2009; *Cappa and Jimenez*, 2010]. The contribution of these semivolatile emissions to ambient particulate matter concentrations will vary with changing atmospheric conditions due to perturbations to thermodynamic equilibrium. However, few studies have quantitatively constrained the gas-particle partitioning of biomass-burning POA, which is essential for updating emissions inventories and chemical transport models to account for its semivolatile nature.

[3] Gas-particle partitioning of atmospheric organics is a sorptive process; vapors can *ab*sorb into organic solution or *ad*sorb onto the surface of soot, mineral dust, and other solid substrates, while dissolution of organics into aqueous
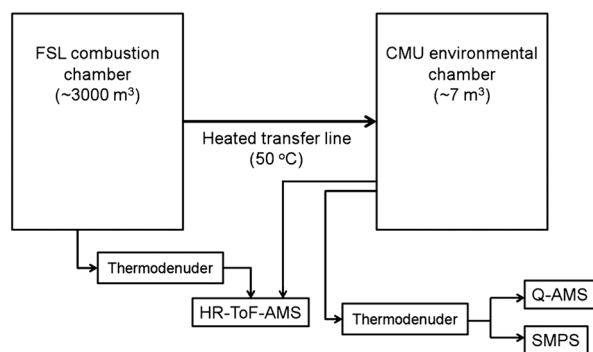
Figure 1. Experimental setup for gas-particle partitioning experiments during the FLAME-III campaign. Fuels were combusted and the smoke was held in the FSL combustion chamber.

particles can also affect gas-particle partitioning. The relative contributions of these mechanisms depend on the amount of sorptive material present. In the atmosphere, *ab*sorption into an organic solution is generally thought to be the primary partitioning mechanism [*Liang et al.*, 1997; *Roth et al.*, 2005; *Arp et al.*, 2008]. Therefore, at phase equilibrium, the POA emission factor (EF$_{OA}$) and the mass fraction of total lower volatility organic emissions residing in the particulate phase (X_p) can be expressed as

$$X_p = \frac{EF_{OA}}{EF_{tot}} = \sum_i f_i \left(1 + \frac{C_i^*(T)}{C_{OA}}\right)^{-1} \quad (1)$$

where $C_i^*(T)$ is the effective saturation concentration of species i at temperature T (related to liquid saturation vapor pressure), C_{OA} is the OA concentration, EF$_{OA}$ is the emission factor for OA (e.g., g OA kg-dry-fuel-consumed^{-1}), f_i is the mass fraction of species i, and EF$_{tot}$ is the emission factor of all lower volatility organics (OA and organic vapors).

[4] Traditional source tests often estimate EF$_{OA}$ by collecting samples on quartz filters and then relating the measured OA mass to the mass of fuel consumed (e.g., g OA kg-fuel^{-1}) [*Andreae and Merlet*, 2001; *Hays et al.*, 2002; *McMeeking et al.*, 2009]. Quartz filters capture particle-phase organics as well as a fraction of the organic vapors that adsorb to the filter (positive-sampling artifact) [*Turpin et al.*, 2000]. *Lipsky and Robinson* [2006] determined that as much as 70% of the total organic carbon (OC) collected on a bare quartz filter can be a sampling artifact (i.e., adsorbed vapors), depending on dilution conditions. Furthermore, there may be a partitioning bias in source test data because C_{OA} during source tests is often much greater than ambient conditions, which shifts gas-particle partitioning toward the particle phase following equation (1) [*Robinson et al.*, 2010]. *Robinson et al.* [2010] estimate that as much as 80% of the OC collected on a quartz filter during traditional source testing may exist as vapors at ambient conditions due to a combination of positive-sampling artifacts and partitioning biases associated with high C_{OA}. In other words, existing emissions inventories may overestimate the contribution of biomass-burning POA emissions to ambient particulate matter concentrations, as a substantial fraction of the semivolatile organic material will likely evaporate with dilution during transport away from the source. To account for the variability in the gas-particle partitioning of the POA emissions, the volatility distribution (set of f_i) of the organics

collected on the quartz filter (which are typically used to define POA emission factors) must be known. Equation (1) can then be used to calculate the POA emission factor or POA concentration at any atmospheric condition (accounting for differences in C_{OA} and/or T).

[5] In theory, volatility distributions can be derived from composition measurements. However, the majority of the lower volatility organics that contribute to POA are not resolvable on a molecular level with traditional analytical instrumentation [*Rogge et al.*, 1998; *Schauer et al.*, 2001]. Furthermore, the saturation concentration (i.e., saturation vapor pressure) of identified compounds may not be known. Therefore, equation (1) is typically applied semiempirically using a surrogate set of compounds that reproduce the gas-particle partitioning of the bulk POA [*Donahue et al.*, 2006; *Robinson et al.*, 2010]. These surrogate compounds are often represented using a one-dimensional volatility basis set [*Donahue et al.*, 2006], which distributes lower volatility organics (here defined as all organics having $C_i^* \leq 3 \times 10^6$ μg m^{-3}) over a logarithmically spaced set of bins of C_i^*. The volatility basis set enables the simulation of gas-particle partitioning of all organic emissions without complete molecular identification.

[6] Few studies have quantified volatility distributions for biomass-burning POA emissions. *Grieshop et al.* [2009] report a volatility distribution for wood smoke emitted from a small stove, while *Cappa and Jimenez* [2010] derive volatility distributions for open biomass-burning OA inferred from factor analysis of ambient and thermally denuded OA from Mexico City. However, it is unclear whether these parameterizations are applicable to fresh open biomass burning or whether they capture the variability associated with different fuels and burning conditions.

[7] The objectives of the laboratory study described here and in Levin et al. (manuscript in preparation) are as follows: Q1 (1) to systematically investigate the gas-particle partitioning of biomass-burning POA emissions from a variety of fuels using thermodenuder and dilution measurements and (2) to derive volatility distributions and EF$_{tot}$ to predict this partitioning across the entire range of atmospheric conditions. This work focuses on thermal perturbations of gas-particle partitioning, while Levin et al. (manuscript in preparation) focus on dilution-based perturbations. The derived parameterizations are designed to update existing biomass-burning PM emissions inventories and chemical transport models to account for semivolatile POA.

2. Experimental Methods

2.1. Overview

[8] Experiments were conducted to investigate the gas-particle partitioning of POA emissions from laboratory fires during the third Fire Lab at Missoula Experiment (FLAME-III) at the U.S. Forest Service Fire Science Laboratory (FSL) in Missoula, MT during September–October 2009. FLAME-III investigated an array of fuels associated with prescribed burning and wildfires in North America (Table S1). Additional description of the experimental setup is presented by *Hennigan et al.* [2011]. This paper focuses on gas-particle partitioning measurements made using the sampling configuration and instruments shown schematically in Figure 1.

2

[9] Briefly, during each experiment, a small mass of fuel (0.3–1.0 kg) was ignited electrically inside the FSL combustion chamber (3014 m^3) and allowed to burn to completion, filling the room with smoke. After allowing roughly 30 min for mixing, samples were then drawn from the FSL combustion chamber to characterize the emissions. Gas-particle partitioning was investigated by heating the sample in a thermodenuder and by dilution. Volatility distributions were derived by fitting the thermodenuder data; predictions based on these fits were then evaluated by comparing the predictions to the dilution data.

2.2. Emission Factors

[10] Emission factors were calculated using a carbon mass balance approach [*Andreae and Merlet*, 2001]:

$$EF_i = \frac{\Delta C_i X_c}{\Delta CO_2 + \Delta CO + \Delta PM_c + \Delta THC} \quad (2)$$

where ΔC_i is the background-corrected pollutant concentration (e.g., organic aerosol and total organics) and X_c is the mass fraction of carbon in the fuel (assumed to be ~0.5 based on *McMeeking et al.* [2009]). The terms in the denominator are the background-corrected CO_2 (LiCor Biosciences Model 820), CO (Teledyne-API Model 400A), carbonaceous PM (OC + elemental carbon, EC; Sunset Laboratories Lab OC-EC Aerosol Analyzer) and total hydrocarbons (THC; from Thermo Environmental Model 51 analyzer using flame ionization detection) concentrations expressed on a carbon mass basis (kg-C m^{-3} for all terms).

2.3. Dilution Measurements

[11] Two different types of dilution data are considered here. First, smoke concentrations inside FSL combustion chamber were slowly diluted over a period of several hours by infiltration of outside air, as the combustion chamber is a large room that is not air tight. The OA concentrations in the outside air were very low ($< 2\ \mu g\ m^{-3}$); therefore, this infiltration reduced the concentrations of the POA in burn chamber by a factor of 5 to 10 over the course of the experiment (~3 h). The median temperature within the laboratory was 21.4°C with a range of 11.1–29.1°C.

[12] Second, the smoke was also diluted by transferring it from the FSL combustion chamber into the Carnegie Mellon University (CMU) portable Teflon® environmental chamber (~7 m^3) using injector diluters (Dekati DI-1000). This was done after the smoke had become well mixed in the FSL chamber (roughly 30 min after completion of the fire) [*Hennigan et al.*, 2011]. After filling, the smoke inside the CMU chamber was a factor of ~25 to 35 more dilute than smoke inside the FSL combustion chamber, inducing evaporation of semivolatile organic material. This dilution into the sealed CMU chamber was performed using dried, HEPA- and activated-carbon-filtered air to minimize the introduction of any background organic material.

[13] OA concentrations in the FSL chamber were measured using a high-resolution time-of-flight aerosol mass spectrometer (HR-ToF-AMS; Aerodyne Research, Inc.) [*DeCarlo et al.*, 2006]. Changes in partitioning due to dilution via infiltration of outside air were characterized using the measured OA-to-sulfate ratio:

$$EF_{OA,\,t} = EF_{OA,\,t=0} \left[\frac{Org}{SO_4^{2-}}\right]_{t=0} \left[\frac{Org}{SO_4^{2-}}\right]_t^{-1} \quad (3)$$

where $EF_{OA,t=0}$ is the initial OA emission factor, $EF_{OA,t}$ is the OA emission factor at time t, and the Org:SO_4^{2-} terms are the OA-to-sulfate ratio at the initial time ($t=0$) and time t. Equation (3) corrects for both dilution and particle wall loss to the chamber walls, assuming sulfate and organic aerosol mass are lost at the same rate. Dilution via infiltration is described in detail in Levin et al. (manuscript in preparation).

[14] Nonrefractory, submicron aerosol mass inside the CMU chamber was characterized using both an HR-ToF-AMS and an Aerodyne quadrupole aerosol mass spectrometer (Q-AMS) [*Canagaratna et al.*, 2007]; collection efficiency in the AMS was assumed to be in unity [*Hennigan et al.*, 2011; *Heringa et al.*, 2011]. Particle size distributions were measured using a scanning mobility particle sizer (SMPS; TSI 3081/3722; TSI, Inc.). The evolution of EF_{OA} with dilution from the FSL chamber to the CMU chamber was also tracked using the change in the OA-to-sulfate ratio measured by the HR-ToF-AMS (equation (3)). The CMU chamber was located outdoors and not temperature controlled. Its median temperature was 9°C with a range of ~1–20°C.

2.4. Thermodenuder Measurements

[15] Two thermodenuders (TD) were used to investigate the effects of heating on gas-particle partitioning; one TD-perturbed OA sampled from the FSL chamber and the other perturbed OA sampled from the CMU chamber. Briefly, a TD is a heated tube followed by a room temperature activated carbon denuder to strip the evaporated organic vapors to minimize recondensation [*Huffman et al.*, 2008]. Both TDs were based on the design of *Huffman et al.* [2008]. Additional information on the TD sampling from the CMU chamber can be found in the supporting information.

[16] To characterize the extent of evaporation in the TD, the aerosol was alternately sampled through the TD and a bypass line maintained at ambient temperature. TD data are presented as the mass fraction remaining (MFR) in the particle phase:

$$MFR = \frac{C_{TD}}{C_{bypass}} \quad (4)$$

where C_{TD} and C_{bypass} are the OA concentrations measured downstream of the thermodenuder and bypass line, respectively. The HR-ToF-AMS was used to measure the OA downstream of the FSL combustion chamber TD; the Q-AMS was used to measure the OA downstream of the CMU chamber TD. The TD sampling directly from the FSL chamber scanned from 30 to 120°C with a centerline residence time (t_{res}) of 13.9 sec at 25°C; the TD sampling from the CMU chamber was operated at fixed temperatures of 40, 80, and 120°C at two t_{res} (18.6 and 6.2 sec). TD data were corrected for particle number losses (mainly due to thermophoresis) using a laboratory calibration performed with ammonium sulfate particles; losses ranged from ~5 to 15% as a function of temperature (for additional details, see the supporting information). No systematic comparison between the two AMS was performed during this

study as much of the time when the HR-ToF-AMS was sampling from the CMU chamber coincided with the Q-AMS sampling through the CMU TD, complicating a direct comparison.

3. Interpreting Gas-Particle Partitioning Data

[17] A major goal of this work was to derive a volatility distribution to describe the gas-particle partitioning data. If the aerosol is in phase equilibrium, a volatility distribution can be derived by fitting equation (1) to the gas-particle partitioning data; if the aerosol is not in equilibrium, then a kinetic model must be used to interpret the data. The equilibration time scale τ for an aerosol can be approximated as the inverse of the condensation sink (CS) [*Seinfeld and Pandis*, 2006]:

$$\tau = CS^{-1} = \left(2\pi d_p N_t DF\right)^{-1} \tag{5a}$$

$$F = \frac{1 + Kn}{1 + 0.3773Kn + 1.33Kn\frac{1+Kn}{\alpha}} \tag{5b}$$

where d_p is the mass-median particle size, N_t is the total aerosol number concentration, D is the diffusion coefficient for the organic vapors in air (assumed to be 5×10^{-6} m^2 s^{-1}) [*Riipinen et al.*, 2010], and F is the Fuchs-Sutugin correction factor, which accounts for non-continuum effects. Kn is the Knudsen number ($= 2\lambda/d_p$, where λ is the mean free path of organic molecules in air at 1 atm and 25°C and taken to be 65.2 nm), and α is the mass accommodation coefficient.

[18] *Saleh et al.* [2011] recommended that a system should be considered to be in equilibrium only if the ratio of $t_{res}/\tau > 5$. If α is greater than or equal to 0.1, this criterion was met for all of the FSL combustion chamber data and most CMU environmental chamber data. The FSL chamber was slowly diluted over a period aerosol several hours versus τ values of ~0.5–25 sec if $\alpha = 1$ and ~3–170 sec if $\alpha = 0.1$. The smoke was allowed to equilibrate in the CMU chamber for 30 min before sampling versus τ values of ~0.5–5 min for $\alpha = 1$ and ~4–26 min for $\alpha = 0.1$. If the aerosol had not equilibrated in the CMU chamber prior to characterization, then our analysis will underestimate the volatility of the biomass-burning POA.

[19] The relatively short residence times within the TD suggest that the aerosol likely did not achieve gas-particle equilibrium ($t_{res}/\tau < 5$). Consequently, the TD data were analyzed using the evaporation kinetics model developed by *Riipinen et al.* [2010], rather than the equilibrium model presented in equation (1). This model tracks both particle- and gas-phase concentrations in each VBS bin i:

$$\frac{dC_{p,i}}{dt} = -CS\left(X_{m,i}Ke_iC_i^* - C_{g,i}\right) \tag{6a}$$

$$\frac{dC_{g,i}}{dt} = -\frac{dC_{p,i}}{dt} \tag{6b}$$

where $C_{p,i}$ is the particle-phase concentration of i, $C_{g,i}$ is the gas-phase concentration of i, $X_{m,i}$ is the mass fraction of i in the particle phase, and Ke_i accounts for the changes in saturation concentration (vapor pressure) due to the surface curvature of the particle. Expressions defining $X_{m,i}$ and Ke_i are provided in the supporting information. These equations were used to model only the heated section of the TD, and the aerosol entering the TD was assumed to be in phase equilibrium.

[20] Recondensation [e.g., *Cappa*, 2010; *Fuentes and McFiggans*, 2012] or evaporation in the denuder [*Cappa and Wilson*, 2011] can complicate the analysis of TD data. We did not consider either of these phenomena in the analysis. *Saleh et al.* [2011] argue that there is little perturbation to the aerosol in the denuding section. Although no measurements were made through the TD at room temperature, only 10% of the OA has evaporated at $T = 30$–40°C, suggesting that evaporation in the denuding section was not very significant (see Figure 3a below). If recondensation occurred in the TD, then our derived volatility distributions will be less volatile than the true distribution. In other words, we would be underestimating evaporated OA mass.

[21] The TD data were collected at three different residence times to investigate the mass accommodation coefficient (α). Recent work has suggested that α may be less than unity for oxidized organic aerosol. *Saleh et al.* [2012] estimated α of ambient OA ranging from 0.28 to 0.46, while Cappa and colleagues have determined that $\alpha > 0.01$ using laboratory-generated and ambient OA [*Cappa and Jimenez*, 2010; *Cappa and Wilson*, 2011].

4. Experimental Results

[22] Partitioning theory (equation (1)) indicates that gas-particle partitioning of semivolatile organics depends on C_{OA}. To investigate the variation of EF$_{OA}$ with C_{OA}, measurements were performed at different levels of dilution using both the FSL and CMU chambers. Emissions data from both chambers are presented in Figure 2 as partitioning plots (EF$_{OA}$ versus C_{OA}). Figure 2a highlights data from two experiments (Burns 38 and 57); Figure 2b compiles data from all of the different burns. Closed markers represent single scans from the HR-ToF-AMS sampling from the FSL chamber, while open markers represent data averaged over 1 h from the Q-AMS sampling from the CMU chamber. The initial EF$_{OA}$ was calculated immediately after the emissions became well mixed inside the entire FSL combustion chamber using equation (2). This corresponds to the highest EF$_{OA}$ (i.e., $t = 0$) for each experiment. The changes in partitioning with dilution were then tracked using the organic-to-sulfate ratio (equation (3)) for both the FSL and CMU chamber. The organic-to-sulfate ratio isolates the changes in gas-particle partitioning by correcting the data for both dilution and particle losses to the chamber walls.

[23] Figure 2 indicates that the combination of the two chambers enabled EF$_{OA}$ measurements for the same burn to be made over a very wide range of C_{OA}. The median initial C_{OA} inside the FSL combustion chamber was ~500 μg m^{-3} with a range from ~100 to 5000 μg m^{-3}. This is much higher than typical ambient concentrations but comparable to those in fire plumes. Infiltration of outside air then reduced the C_{OA} inside the FSL chamber by a factor of 5 to 10 over the course of the experiment (roughly 3 h). C_{OA} inside the CMU chamber ranged from 5 to 50 μg m^{-3} (25 to 35 times lower than the initial, well-mixed conditions inside the FSL combustion chamber). Therefore, the CMU chamber data are representative of ambient conditions.

[24] Two conclusions can be drawn from Figure 2. First, as expected, a very wide range of EF$_{OA}$ values were measured across the set of experiments with values ranging from ~0.5 to ~300 g OA kg-dry-fuel^{-1} based on the AMS measurements.
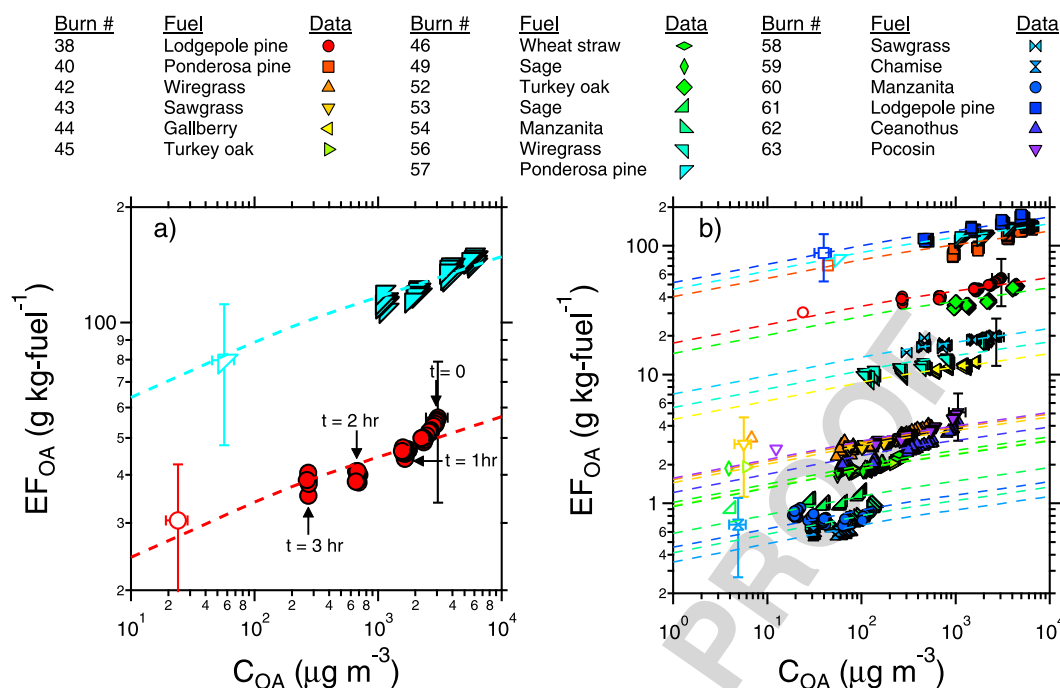
Burn #	Fuel	Data	Burn #	Fuel	Data	Burn #	Fuel	Data
38	Lodgepole pine	●	46	Wheat straw	◆	58	Sawgrass	⋈
40	Ponderosa pine	■	49	Sage	◆	59	Chamise	✕
42	Wiregrass	▲	52	Turkey oak	◆	60	Manzanita	●
43	Sawgrass	▼	53	Sage	◢	61	Lodgepole pine	■
44	Gallberry	◀	54	Manzanita	◣	62	Ceanothus	▲
45	Turkey oak	▶	56	Wiregrass	◥	63	Pocosin	▼
			57	Ponderosa pine	◤			

Figure 2. Organic aerosol emission factor (EF$_{OA}$) as a function of organic aerosol concentration (C_{OA}) measured during the FLAME-III campaign for (a) Burn 38 (lodgepole pine) and burn 57 (ponderosa pine); (b) all burns. Closed markers represent data measured in FSL combustion chamber, while open markers represent data measured in the CMU environmental chamber. Dashed lines represent model predictions based on the parameters recommended for ambient gas-particle partitioning in Table 2; the coloration is identical to the experimental data. Representative measurement uncertainty is provided for a subset of the data.

This variability is consistent with the large body of biomass-burning emissions data [*Andreae and Merlet*, 2001; *Hays et al.*, 2002; *McMeeking et al.*, 2009]. It reflects the fact that biomass-burning emissions depend on fuel composition and combustion conditions. These experiments did not control for combustion phase or intensity, and a wide range of combustion conditions occurred including primarily flaming fires versus primarily smoldering fires, driven by fuel type and fuel moisture content. The highest-emitting fuels (~100–300 g OA kg-dry-fuel^{-1}) had high water contents leading to less efficient combustion [*Watson et al.*, 2011]. The fire-integrated modified combustion efficiency and emission factors are listed in the supporting information.

[25] The second important conclusion shown in Figure 2 is that, for a given burn, the measured EF$_{OA}$ decreased with decreasing C_{OA}. For example, Figure 2a shows that dilution from the FSL combustion chamber into the CMU environmental chamber reduced EF$_{OA}$ by roughly a factor of 2 (the CMU data roughly correspond to the $t = 0$ FSL data point). Figure 2b shows that this trend was observed across the entire set of experiments. However, in two burns, similar EF$_{OA}$ was measured in both the CMU and the FSL chamber (e.g., burns 42 and 53). This may be observed because the CMU chamber was roughly 10°C colder than the FSL chamber, which promotes recondensation of organic vapors that evaporated during dilution.

[26] The TD data provide additional evidence that a significant fraction of the POA emissions are semivolatile. Both the FSL and CMU chamber TD data are presented in **F3** Figure 3a. In every experiment, the POA evaporated (i.e., MFR decreased) with heating; for example, roughly 20% of the POA evaporated with heating to 40°C. Significant evaporation was observed with heating at both ambient- (C_{OA} ~5 µg m^{-3}) and plume-like concentrations (C_{OA} ~500 µg m^{-3}). This demonstrates that POA is semivolatile over a wide range of conditions. There was some scatter in the TD data which was largely due to differences in C_{OA} and particle size (see equations (5)–(6)). Some MFR values were slightly greater than unity (the theoretical maximum) due to low Q-AMS signal-to-noise at low C_{OA}.

[27] The extent of evaporation (MFR) did not vary strongly with residence time. For example, in the CMU TD, the median value of MFR at 80°C was 0.53 for the long t_{res} (18.6 sec) versus 0.61 for the short t_{res} (6.2 sec), thus having a relative percent difference of ~14%. If $\alpha = 1$ or 0.1, then equation (6) predicts a relative percent difference of ~17% and ~12% between the two residence times for values of $\alpha = 1$ and 0.1, respectively. As α become smaller, the difference in MFR between the two residence times decreases since the evaporation rate is slower (e.g., for $\alpha = 0.01$, the relative percent difference between the two t_{res} is ~5%). This suggests that there was little mass transfer resistance to evaporation inside the TD, provided that ΔH_{vap} was similar to that recently inferred for aerosol mixtures [e.g., *Grieshop et al.*, 2009; *Ranjan et al.*, 2012] rather than pure components [e.g., *Epstein et al.*, 2010]. A similar conclusion is implied by the lack of a plateau in the thermograms in Figure 3a [e.g., *Cappa and Jimenez*, 2010].

[28] Figures 2 and 3 clearly demonstrate that a large fraction of the POA is semivolatile. The large, systematic changes in gas-particle partitioning over a wide range of measured C_{OA} and temperature implies a broad distribution of organic compound volatilities. Finally, the similarity in the
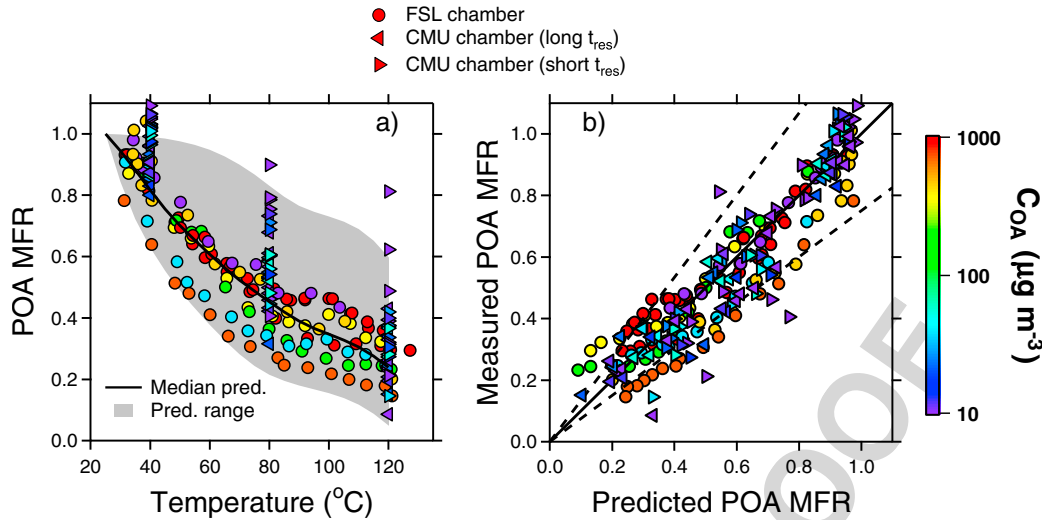
Figure 3. (a) Thermodenuder data collected during the FLAME-III campaign—mass fraction remaining (MFR) versus thermodenuder temperature. (b) Comparison of measured and predicted POA MFR using the parameters from Table 2. Different markers represent the three different sampling configurations. Data are compared to model predictions using the parameters listed in Table 2 with the median experimental C_{OA} and d_p (solid line) as well as the entire range of C_{OA} and d_p (gray region in Figure 3a). Dashed lines in Figure 3b represent experimental uncertainty of $\pm 30\%$ (propagated from AMS and SMPS uncertainty provided in the text). The logarithmic color scale saturates at 1000 µg m^{-3}.

partitioning behavior (i.e., similar $\Delta EF_{OA}/\Delta C_{OA}$ or $\Delta MFR/\Delta T$) across the set of experiments using different fuels suggests that a single-volatility distribution may be adequate to predict the gas-particle partitioning of the entire data set.

5. Inferring Volatility Distributions From the Thermodenuder Data

[29] In this section, a single set of partitioning parameters (f_i, $\Delta H_{vap,i}$ and α) is presented to represent all of the TD data. These parameters were derived by fitting equation (6) to all of the TD data presented in Figure 3a. These data span a broad range of conditions—C_{OA} (~1–5000 µg m^{-3}) and T (~30–120°C)—enabling the fits to constrain the volatility distribution over a wide range of C_i^* values (10^{-2} to 10^4 µg m^{-3}). Therefore, the derived parameterizations are constrained by data across both plume- and ambient-like conditions. All of the TD data were fit simultaneously since there appears to be only modest experiment-to-experiment differences in gas-particle partitioning behavior.

[30] Since $\Delta H_{vap,i}$ and α are generally unknown a priori, uniqueness is a major problem when fitting TD data [*Cappa and Jimenez*, 2010]; that is, the TD data can be equivalently described using multiple combinations of partitioning parameters (f_i, $\Delta H_{vap,i}$ and α). To investigate this issue, solutions for a set of volatility distributions were derived by fitting the entire TD data set using different combinations of $\Delta H_{vap,i}$ and α. The fitting was performed using a brute-force algorithm that systematically considered a large number (9900) of combinations of f_i, $\Delta H_{vap,i}$, and α. The evaporation kinetics model of *Riipinen et al.* [2010] was then used to calculate the extent of evaporation (MFR) for each combination of inputs ($\Delta H_{vap,i}$, α, and f_i). The model performance for each combination of inputs was assessed by computing the sum of the square of the residuals (SSR) between measured and predicted MFR.

[31] The 9900 different combinations of input parameters for the brute-force fitting are summarized in Table 1. The **T1** goal was to consider a wide, but physically realistic range, in each parameter. First, a log linear relationship was assumed between $\Delta H_{vap,i}$ and C_i^* [*Epstein et al.*, 2010]. The range of slope and intercept values for this relationship is listed in Table 1; they were defined based on results from *Grieshop et al.* [2009] and *Epstein et al.* [2010]. There is similar uncertainty in the value of α [*Kolb et al.*, 2010]. In the literature, α is generally assumed to be in unity; however, recent studies have suggested that α may have values between 0.01 and 1 [*Saleh et al.*, 2009; *Cappa and Jimenez*, 2010; *Lee et al.*, 2010; *Riipinen et al.*, 2010; *Saleh et al.*, 2012]. Therefore, the calculations were performed with α values of 1, 0.1, and 0.01. While the actual value of α may fall in between these logarithmically spaced values, the different partitioning parameters are correlated. In other words, the effects of changing α can be compensated for, to some extent, by adjusting $\Delta H_{vap,i}$ and f_i. Therefore, without additional constraints, the fitting procedure cannot provide a highly refined value of α. The range of α considered here does provide some insight into the importance of mass transfer resistance.

Table 1. Parameter Ranges Used for Brute-Force Fitting

ΔH_{vap} intercept (kJ mol^{-1})	ΔH_{vap} slope (kJ mol^{-1})	α
70, 85, 100, 115, 130	4, 6, 8, 11	0.01, 0.1, 1

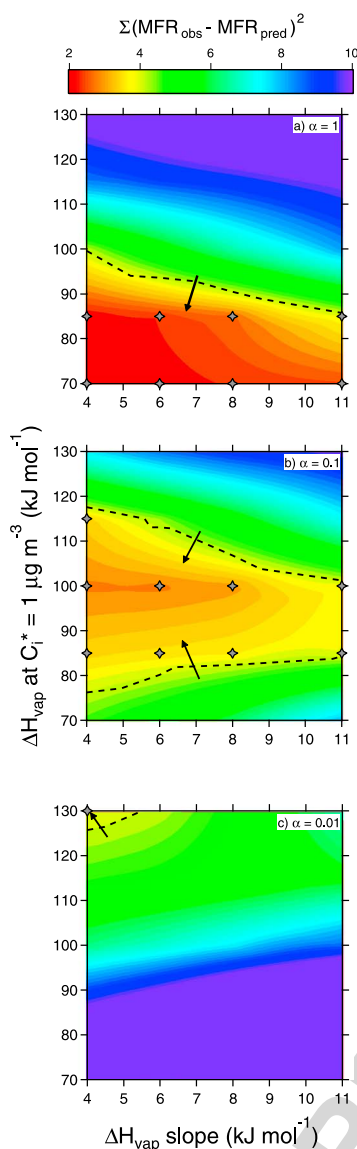| log C^* (µg m^{-3})	Minimum f_i value	Maximum f_i value
-2	0.1	0.2
-1	0	0.2
0	0	0.3
1	0	0.3
2	0.1	0.3
3	0.1	0.4
4	0.3	0.7

Figure 4. Contour plots of the sum of the squared residuals as a function of the slope (*x* axis) and intercept (*y* axis) of relationship between ΔH_{vap} and C* for three values of α: (a) $\alpha = 1$, (b) $\alpha = 0.1$, and (c) $\alpha = 0.01$. Solutions falling within experimental uncertainty are bounded by the dashed lines; arrows point into the region of statistically acceptable solutions. Contour colors are saturated at a value of 10. Model outputs falling within experimental uncertainty are indicated by the markers. Only the best solution for each combination has been shown; there are many other solutions associated with these combinations that yield statistically acceptable fits (see Figure S2).

[32] For each combination of $\Delta H_{vap,i}$ and α, model calculations were performed for 165 different volatility distributions defined between the upper and lower bounds listed in Table 1. These bounds were defined based on a preliminary analysis using a subset of the data from the CMU TD. In this preliminary analysis, it was determined that there must be some mass in the $C_i^* = 10^{-2}$ μg m^{-3} bin; hence, the minimum value of this bin was constrained to be nonzero. In the atmosphere, material in this $C_i^* = 10^{-2}$ μg m^{-3} bin will

essentially always be in the particle phase, so any less volatile material ($C_i^* < 10^{-2}$ μg m^{-3}) is incorporated into this bin.

[33] Other inputs for the model were the experimentally measured mass-median d_p (using the SMPS) and C_{OA} (from the HR-ToF-AMS or Q-AMS). Size distributions were not measured in FSL combustion chamber; therefore, we used the particle size distributions measured in the CMU environmental chamber for all of the analyses. This assumption is not strictly valid because dilution causes the particles to shrink when they are transferred from the FSL combustion chamber to the CMU environmental chamber. However, additional processes such as coagulation complicate extrapolating the CMU chamber size data back to the FSL chamber. Therefore, we assume that growth due to coagulation will roughly offset shrinkage due to evaporation, although in reality, the particle size distributions are likely different. Finally, values of D, σ, ρ, and MW$_i$ were taken from the literature (summarized in Table S2); prior work has demonstrated that the model is not overly sensitive to these parameters [*Riipinen et al.*, 2010; *Fuentes and McFiggans*, 2012].

[34] SSR values for all 9900 different combinations of input parameters are presented in Figure 4 as contours that are a function of the assumed slope (*x* axis) and the assumed intercept for the log linear ΔH_{vap} relationship (*y* axis) as well as α (different panels). An acceptable solution was defined as one that described the experimental data within experimental uncertainty. Using the measurement uncertainties (estimated to be $\pm 20\%$ (1σ) for the measured mass concentrations in the AMS [*Bahreini et al.*, 2009] and $\pm 10\%$ for measured diameters in the SMPS based on product literature), a threshold value of 4.18 for the maximum SSR was defined for an acceptable solution (see supporting information for additional information). **F4**

[35] A large number (441 out 9900) of the combinations of f_i, $\Delta H_{vap,i}$, and α describe the entire set of TD data within the experimental uncertainty. Therefore, there is no single unique solution. The dashed line in Figure 4 encloses the range of $\Delta H_{vap,i}$ and α for which at least one of the input volatility distributions yielded an SSR value less than the experimental uncertainty. For most of these combinations, multiple acceptable distributions have been found, as shown in Figure S2; the symbols indicate the minimum SSR for a given combination of $\Delta H_{vap,i}$ and α.

[36] Figure 4 suggests that $\Delta H_{vap,i}$ and α were strongly correlated; for example, low values of $\Delta H_{vap,i}$, were required when $\alpha = 1$ versus higher values when $\alpha < 1$. However, the values of $\Delta H_{vap,i}$ that yield statistically acceptable fits were lower than those of pure components (based on the semi-empirical correlation of *Epstein et al.* [2010]). This ΔH_{vap} lowering was likely an artifact of the representation of the partitioning behavior of thousands of organic compounds using seven surrogate species [*Donahue et al.*, 2006]. Finally, for the ranges of the parameters considered in this analysis (Table 1), mass transfer limitations do not appear to be significant because only 0.4% of the statistically acceptable solutions from the input parameter space were found for $\alpha = 0.01$. Obtaining additional solutions for $\alpha = 0.01$ requires physically unrealistic values of ΔH_{vap} (values greater than that from pure components based on *Epstein et al.* [2010]).

[37] The best fit (lowest SSR) volatility distribution and associated $\Delta H_{vap,i}$ derived for biomass-burning POA emissions are listed in Table 2. This entire set of parameters (f_i, $\Delta H_{vap,i}$ and α) must be used together to describe partitioning **T2**

Table 2. Recommended Volatility Distribution for Biomass-Burning POA Emissions ($\alpha = 1$, $\Delta H_{vap} = 85 - 4 \log C_i^*$)

$\log C_i^*$ (@ 298K)	f_i
−2	0.2
−1	0.0
0	0.1
1	0.1
2	0.2
3	0.1
4	0.3

data (i.e., if $\Delta H_{vap,i}$ or α are changed, the data must be refit to find a new set of f_i). The best solutions for $\alpha = 0.1$ and $\alpha = 0.01$ are provided in Table S3 in the supporting information.

[38] Figure 3a compares the best fit volatility distribution to the experimental data. The solid line is the prediction using the median observed values of C_{OA} and d_p, while the gray region shows the range of predictions for all possible combinations of measured C_{OA} and d_p. Almost all of the data are bounded by the gray region, suggesting that the $\alpha = 1$ solution captures most of the variability in the observed MFR data by simply accounting for variations in C_{OA} and d_p.

[39] Figure 3b provides a more robust assessment of the goodness of fit. It presents a scatterplot of measured versus calculated MFR. The best fit set of parameters listed in Table 2 reproduced more than 95% of the TD data within the experimental uncertainty. This demonstrates that a single set of partitioning parameters can reproduce the entire TD data set that included a wide range of fuels and combustion conditions. Figure 3b also demonstrates that the scatter in the TD data shown in Figure 3a was primarily due to differences in C_{OA} and d_p that affect the evaporation rate. Since this parameterization is able to reproduce both the FSL chamber and CMU chamber TD data reasonably well, the recommended parameterization appears robust for describing biomass-burning POA gas-particle partitioning for both plume- and ambient-like conditions.

6. Emission Factors for Lower Volatility Organics (EF_{tot})

[40] This section compares predictions based on partitioning parameters derived from the TD data (Table 2) to the dilution data from both chambers presented in Figure 2. This provides an important, independent test of the proposed set of partitioning parameters because the dilution data were not used to derive the parameters listed in Table 2.

[41] To predict POA emission factors and concentrations, the best fit partitioning parameters listed in Table 2 (f_i, $\Delta H_{vap,i}$, and α) must be combined with an emission factor for lower volatility organics (EF_{tot} in equation (1)). Although a single set of partitioning parameters (f_i, $\Delta H_{vap,i}$, and α) appear to describe all of the data, there were large burn-to-burn variations in EF_{tot}. This is demonstrated by the large range of EF_{OA} shown in Figure 2 (roughly two orders of magnitude separate the lowest-emitting burn and the highest-emitting burn). Therefore, separate values of EF_{tot} were derived for each burn. These were calculated by applying equation (1) to the measured EF_{OA} data in Figure 2 using the best fit volatility distribution listed in Table 2.

[42] The quality of the predictions of EF_{OA} using the parameters in Table 2 is shown in Figure 2. Most of the predictions fall within the uncertainty range of the data (±30%). However, there are some exceptions. Underpredictions of EF_{OA} in the combustion chamber are likely attributed to particle and vapor wall loss (see Levin et al., manuscript in preparation, for more details), while underpredictions of EF_{OA} in the CMU chamber appear to be large due to differences in temperature between the FSL chamber and the CMU chamber, as the median ΔT between the two chambers was ~10°C. One additional factor that could contribute to the systematic bias between the measurements and the model is if the aerosol had not reached equilibrium in the CMU chamber; this could occur if α was less than 0.1. Finally, we are unable to explain the observed behavior of smoke from Burns 53 and 60, during which EF_{OA} increased with dilution. We attribute this increase to experimental uncertainty. Nevertheless, the model representation of the data is generally robust.

[43] A final detail is that the volatility distribution (and EF_{tot}) can only be constrained over the range of the experimental data. The maximum concentrations in the FSL combustion chamber were ~5000 µg m^{-3}, which means that experimental data only provide information on the emission up to a C_i^* value of about 10^4 µg m^{-3} (the maximum volatility bin in Table 2). Therefore, the derived EF_{tot} values can only account for emissions with a C_i^* value less than or equal to ~10^4 µg m^{-3}. We refer to this value of EF_{tot} as EF_{10000}, which corresponds to the emission factor of all lower volatility organics that fall in the $C_i^* = 10^4$ µg m^{-3} and lower bins. This limitation does not affect the utility of the proposed distribution for predicting gas-particle partitioning of the POA because atmospheric (and even plume) C_{OA} are generally orders of magnitude smaller than 10^4 µg m^{-3}. However, vapors having $C_i^* > 10^4$ µg m^{-3} likely contribute to secondary organic aerosol formation [*Robinson et al.*, 2007]; these vapors are not included in the EF_{10000} values derived here.
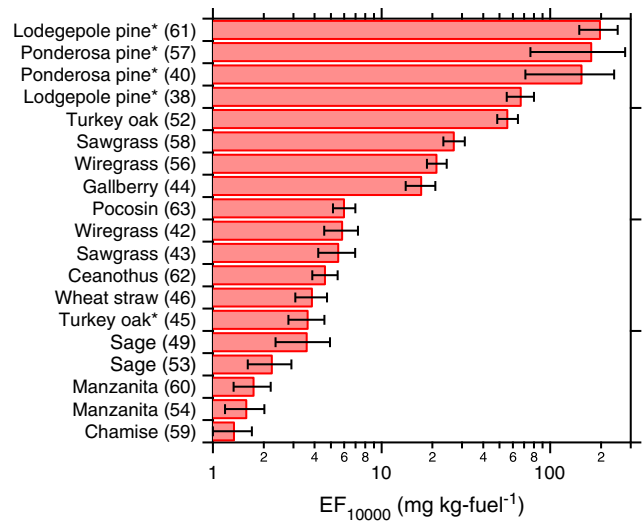

Figure 5. Emission factor of lower volatility organics (EF_{10000}) derived from each experiment. Asterisks indicate high moisture content fuels. Error bars represent one standard deviation in calculated EF_{10000} based on all 441 acceptable solutions.
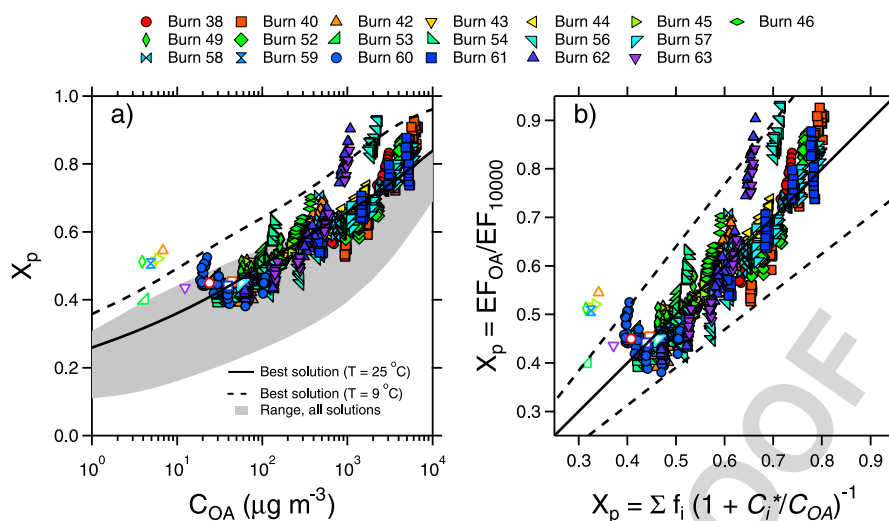
Figure 6. (a) Particle mass fraction (X_p) calculated from the FSL combustion chamber and CMU environmental chamber data, shown as a function of the measured organic aerosol concentrations (C_{OA}). The data are compared to model predictions based on the parameters listed in Table 2 at 25°C (median FSL chamber temperature; solid line) and 9°C (median CMU chamber temperature; dashed line in Figure 6a), and the 441 solutions as constrained by the TD data (shaded region in Figure 6a). (b) Comparison of X_p calculated as the ratio of EF_{OA} to EF_{10000} versus X_p predicted using the summation term in equation (1) at 25°C. The solid line in Figure 6b is the 1:1 line, and the dashed lines are ±30% (experimental uncertainty).

F5 [44] Figure 5 presents the EF_{10000} values for each burn. As expected, they span a wide range, from ~5 g kg-fuel^{-1} to ~500 g kg-fuel^{-1}. The error bars in Figure 5 represent the relative standard deviation (~10–20%) in predicted EF_{10000} for each burn for all 441 statistically acceptable solutions. Direct comparisons of these values to emission factors from literature are complicated because quartz filter measurements are influenced by both partitioning biases and sampling artifacts. Our EF_{10000} are comparable to quartz-filter-derived emission factor values reported in the literature, but it is not known what subset of organics the literature values represent (e.g., EF_{OA} and EF_{10000}).

F6 [45] Figure 6 presents emissions data as particle fractions (X_p; equation (1)) calculated by normalizing EF_{OA} in Figure 2 with the EF_{10000} values in Figure 5. X_p is simply the ratio of EF_{OA} measured with the AMS to EF_{10000} for that burn. This causes all of the data to cluster along a single curve, which demonstrates that the volatility distribution listed in Table 2 provides a reasonable (yet imperfect) representation of measured changes in partitioning with dilution.

[46] The solid line in Figure 6a represents the predicted partitioning using equation (1) and the volatility distribution listed in Table 2 at 25°C. The gray area in Figure 6a indicates the range of predictions based on all 441 statistically acceptable fits. Equilibrium calculations (equation (1)) were performed for comparisons with the chamber data because the best fit solution has an α value of 1, so the OA should be in phase equilibrium (see section 3).

[47] Figure 6b indicates that the model measurement agreement for most points was within ±30% (the experimental uncertainty). The model predictions shown in Figure 6a were not derived by fitting the dilution data. Therefore, this figure provides an independent evaluation of the parameterization. However, the model based on the parameters in Table 2 does not perfectly reproduce the data. The most

notable model measurement discrepancy is the CMU chamber data, most of which falls well outside the error bounds. The CMU chamber data suggest that the aerosol was less volatile than the predictions based on our recommended parameters. However, the CMU chamber was, on average, 10°C colder than the FSL chamber. The base comparison shown in Figure 6 does not account for this temperature difference. Figure 6 also provides a model prediction at the median CMU chamber temperature (9°C; dashed line). Accounting for this temperature difference greatly improves the model performance, shifting the model predictions to within in the experimental uncertainty. Another factor that could potentially contribute to the discrepancy is if the CMU chamber has not reached phase equilibrium (i.e., if $\alpha \leq 0.1$).

[48] These deviations between the model predictions and dilution data must be kept in perspective. First, the proposed volatility distribution provides a much more accurate representation of the data than the assumption of nonvolatile POA (i.e., no change in X_p with C_{OA}). Second, using a single distribution to represent all of the data (albeit imperfectly) has significant advantages over using multiple distributions specific to individual fuels or combustion conditions, even if those other distributions provide slightly improved model performance.

7. Discussion and Atmospheric Implications

[49] Both the thermodenuder and dilution data clearly demonstrated that the majority of the POA emissions from laboratory fires investigated here were semivolatile across a very wide range of atmospheric conditions. The FSL chamber dilution and TD data indicate that both heating and dilution of biomass-burning POA under plume-like conditions cause substantial evaporation. Substantial evaporation was also observed when the biomass-burning POA was under ambient-like
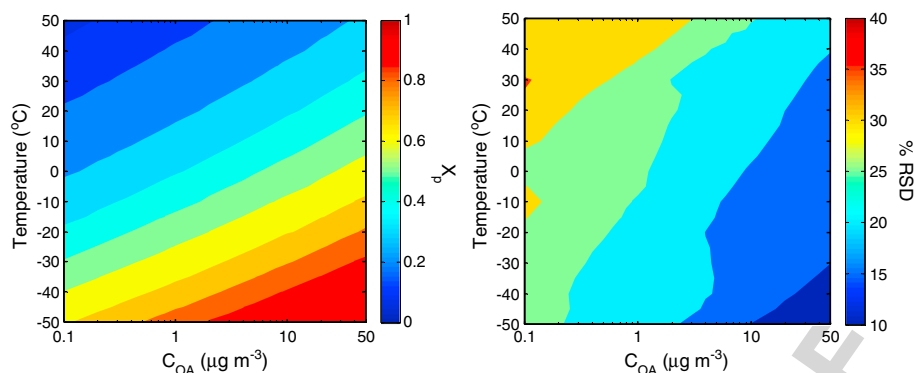
Figure 7. (a) Predicted particle fraction (X_p) for the recommended partitioning parameterization (Table 2) over a wide range of atmospheric conditions. (b) Variability (percent relative standard deviation) in the predicted partitioning for all 441 solutions that describe the data within measurement uncertainty.

conditions inside the CMU chamber. As expected, the total emissions of lower volatility organics (i.e., EF_{tot} representing organic material spanning C_i^* 10^{-2} to 10^4 µg m^{-3}) varied widely with fuel composition and burning conditions. However, essentially all of the partitioning data can be represented (within experimental uncertainty) using a single-partitioning parameterization (f_i, $\Delta H_{vap,i}$ and α).

[50] Given the variability in the composition of biomass smoke [*Fine et al.*, 2001; *Schauer et al.*, 2001; *Fine et al.*, 2002; *McMeeking et al.*, 2009], one might consider the similarity in the measured partitioning behavior across the set of experiments surprising. However, the behavior of the bulk POA is determined by a complex mixture of hundreds of lower volatility organic compounds. When taken together, the overall partitioning behavior of all these mixtures (i.e., the emissions from all biomass fuels considered in this study) was similar enough to be represented reasonably well using a single parameterization. Parameterizations of somewhat higher statistical quality can be achieved if one considers the data from each burn individually. However, in our opinion, the very modest improvements in model performance are not worth the added complexity of having to treat the partitioning behavior of each type of smoke differently. Having one set of parameters simplifies accounting for gas-particle partitioning of biomass-burning POA in emissions inventories and chemical transport models. Although we investigated emissions from 15 fuels over a variety of combustion conditions, additional laboratory or field data are needed to further test the proposed partitioning parameterization across an even broader range of emissions. Furthermore, emissions experiments and inventories must report an emission factor as well as the OA concentration and temperature at which that emission factor was measured in order to account for gas-particle partitioning with atmospheric transport.

[51] Uniqueness complicates the derivation of gas-particle partitioning parameterizations from thermodenuder data. Of the 9900 different combinations of properties considered in this analysis, 441 provided statistically acceptable fits that were within experimental uncertainty. Although all of these fits provide a reasonable representation of the experimental data, an important question is how well constrained the solutions are as one extrapolates away from measurement conditions.

[52] Figure 7a presents X_p calculated using the parameters in Table 2 over a wide range of atmospheric conditions. These calculations were performed using equation (1) by varying C_{OA} and T. Figure 7b provides the percent relative standard deviation (% RSD) of all the different values of X_p across the set of 441 statistically acceptable solutions. From Figure 7, we can draw several conclusions. Gas-particle partitioning (i.e., X_p) varies by more than an order of magnitude across the atmospheric range of C_{OA} and T (Figure 7a). This implies that material present in the particle phase in one part of the atmosphere will likely exist in the gas phase elsewhere (e.g., from the immediate proximity of a fire to an area with lower biomass-burning emissions) and vice versa (e.g., with undiluted lifting of a biomass-burning plume to the colder free troposphere by dry convection). Therefore, inventories and models need to explicitly account for gas-particle partitioning of biomass-burning POA.

[53] As expected, the partitioning predictions from the set of statistically acceptable solutions diverge (i.e., % RSD increases in Figure 7b) as we extrapolate away from the experimental conditions ($C_{OA} \approx 5$–50 µg m^{-3}) toward more dilute conditions ($C_{OA} \approx 0.1$–1 µg m^{-3}). Fortunately, the differences among the set of 441 solutions was relatively small across a wide range of atmospheric conditions (% RSD $\approx$ 10–30%). Therefore, all of the acceptable solutions predict similar atmospheric behavior. Furthermore, the variability across the set of solutions (%RSD < 30%) was much less than the changes in gas-particle partitioning across the range of atmospheric conditions (more than a factor of 10), suggesting that all solutions could be used interchangeably with similar results.

[54] Figure 7a also demonstrates the predicted sensitivity of gas-particle partitioning of biomass-burning POA to changes in temperature and concentration over a wide range of atmospheric conditions. Within the range of $C_{OA} = 0.5$–30 µg m^{-3} (OA levels in the Northern Hemisphere) [*Zhang et al.*, 2007], isothermal dilution causes X_p to change by ~2.5% (µg m^{-3})$^{-1}$. X_p is most sensitive to changes in C_{OA} at clean conditions (i.e., at low concentrations). The sensitivity of X_p to changes in temperature is ~0.7% °C^{-1}, between $T = -50$ to 50°C. Consequently, changes in both C_{OA} and T can strongly influence gas-particle partitioning of biomass-burning POA.

F7

10

[55] The lowest volatility bin considered in our analysis was 10^{-2} µg m^{-3}. In reality, organic material having $C_i^* < 10^{-2}$ µg m^{-3} is likely present in the emissions. In the supporting information, we provide an alternate solution extending C_i^* to 10^{-6} µg m^{-3}, which may prove useful for modeling thermal desorption techniques (e.g., from the impactor in the micro-orifice volatilization impactor chemical ionization mass spectrometer) [*Yatavelli et al.*, 2012] or in advanced chemical modeling (new particle formation [*Pierce et al.*, 2011] or atmospheric lifetime using the 2D-VBS [*Donahue et al.*, 2013]). Both the recommended (Table 2) and alternate (Table S4) solutions are derived following the same approach and yield nearly identical results for atmospheric gas-particle partitioning.

References

Andreae, M. O., and P. Merlet (2001), Emission of trace gases and aerosols from biomass burning, *Global Biogeochem. Cycles*, *15*(4), 955–966, doi:10.1029/2000GB001382.

Arp, H. P. H., R. P. Schwarzenbach, and K. U. Goss (2008), Ambient gas/particle partitioning. 1. Sorption mechanisms of apolar, polar, and ionizable organic compounds, *Environ. Sci. Technol.*, *42*(15), 5541–5547, doi:10.1021/es703094u.

Bahreini, R., et al. (2009), Organic aerosol formation in urban and industrial plumes near Houston and Dallas, Texas, *J. Geophys. Res.*, *114*, D00F16, doi:10.1029/2008JD011493.

Bond, T. C., D. G. Streets, K. F. Yarber, S. M. Nelson, J. H. Woo, and Z. Klimont (2004), A technology-based global inventory of black and organic carbon emissions from combustion, *J. Geophys. Res.*, *109*, D14203, doi:10.1029/2003JD003697.

Canagaratna, M. R., et al. (2007), Chemical and microphysical characterization of ambient aerosols with the aerodyne aerosol mass spectrometer, *Mass Spectrom. Rev.*, *26*(2), 185–222, doi:10.1002/mas.20115.

Cappa, C. D. (2010), A model of aerosol evaporation kinetics in a thermodenuder, *Atmos. Meas. Tech.*, *3*(3), 579–592, doi:10.5194/amt-3-579-2010.

Cappa, C. D., and J. L. Jimenez (2010), Quantitative estimates of the volatility of ambient organic aerosol, *Atmos. Chem. Phys.*, *10*(12), 5409–5424, doi:10.5194/acp-10-5409-2010.

Cappa, C. D., and K. R. Wilson (2011), Evolution of organic aerosol mass spectra upon heating: Implications for OA phase and partitioning behavior, *Atmos. Chem. Phys.*, *11*(5), 1895–1911, doi:10.5194/acp-11-1895-2011.

DeCarlo, P. F., et al. (2006), Field-deployable, high-resolution, time-of-flight aerosol mass spectrometer, *Anal. Chem.*, *78*(24), 8281–8289, doi:10.1021/ac061249n.

Donahue, N. M., A. L. Robinson, C. O. Stanier, and S. N. Pandis (2006), Coupled partitioning, dilution, and chemical aging of semivolatile organics, *Environ. Sci. Technol.*, *40*(8), 2635–2643, doi:10.1021/Es052297c.

Donahue, N. M., W. Chuang, S. A. Epstein, J. H. Kroll, D. R. Worsnop, A. L. Robinson, P. J. Adams, and S. N. Pandis (2013), Why do organic aerosols exist? Understanding aerosol lifetimes using the two-dimensional volatility basis set, *Environ. Chem.*, *10*, 151–157, doi:10.1071/EN13022.

Epstein, S. A., I. Riipinen, and N. M. Donahue (2010), A semiempirical correlation between enthalpy of vaporization and saturation concentration for organic aerosol, *Environ. Sci. Technol.*, *44*(2), 743–748, doi:10.1021/Es902497z.

Fine, P. M., G. R. Cass, and B. R. T. Simoneit (2001), Chemical characterization of fine particle emissions from fireplace combustion of woods grown in the northeastern United States, *Environ. Sci. Technol.*, *35*(13), 2665–2675, doi:10.1021/es001466k.

Fine, P. M., G. R. Cass, and B. R. T. Simoneit (2002), Chemical characterization of fine particle emissions from the fireplace combustion of woods grown in the southern United States, *Environ. Sci. Technol.*, *36*(7), 1442–1451, doi:10.1021/es0108988.

Fuentes, E., and G. McFiggans (2012), A modeling approach to evaluate the uncertainty in estimating the evaporation behaviour and volatility of organic, *Atmos. Meas. Tech.*, *5*(4), 735–757, doi:10.5194/amt-5-735-2012. [Q3]

Grieshop, A. P., M. A. Miracolo, N. M. Donahue, and A. L. Robinson (2009), Constraining the volatility distribution and Gas-particle partitioning of combustion aerosols using isothermal dilution and thermodenuder measurements, *Environ. Sci. Technol.*, *43*(13), 4750–4756, doi:10.1021/Es8032378.

Hays, M. D., C. D. Geron, K. J. Linna, N. D. Smith, and J. J. Schauer (2002), Speciation of gas-phase and fine particle emissions from burning of foliar fuels, *Environ. Sci. Technol.*, *36*(11), 2281–2295, doi:10.1021/Es0111683.

Hennigan, C. J., et al. (2011), Chemical and physical transformations of organic aerosol from the photo-oxidation of open biomass burning emissions in an environmental chamber, *Atmos. Chem. Phys.*, *11*(15), 7669–7686, doi:10.5194/acp-11-7669-2011.

Heringa, M. F., P. F. DeCarlo, R. Chirico, T. Tritscher, J. Dommen, E. Weingartner, R. Richter, G. Wehrle, A. S. H. Prevot, and U. Baltensperger (2011), Investigations of primary and secondary particulate matter of different wood combustion appliances with a high-resolution time-of-flight aerosol mass spectrometer, *Atmos. Chem. Phys.*, *11*(12), 5945–5957, doi:10.5194/acp-11-5945-2011.

Huffman, J. A., P. J. Ziemann, J. T. Jayne, D. R. Worsnop, and J. L. Jimenez (2008), Development and characterization of a fast-stepping/scanning thermodenuder for chemically resolved aerosol volatility measurements, *Aerosol Sci. Technol.*, *42*(5), 395–407, doi:10.1080/02786820802104981.

Huffman, J. A., K. S. Docherty, C. Mohr, M. J. Cubison, I. M. Ulbrich, P. J. Ziemann, T. B. Onasch, and J. L. Jimenez (2009), Chemically resolved volatility measurements of organic aerosol from different sources, *Environ. Sci. Technol.*, *43*(14), 5351–5357, doi:10.1021/Es803539d.

Kolb, C. E., et al. (2010), An overview of current issues in the uptake of atmospheric trace gases by aerosols and clouds, *Atmos. Chem. Phys.*, *10*(21), 10,561–10,605, doi:10.5194/acp-10-10561-2010.

Lee, B. H., et al. (2010), Measurement of the ambient organic aerosol volatility distribution: Application during the Finokalia Aerosol Measurement Experiment (FAME-2008), *Atmos. Chem. Phys.*, *10*(24), 12,149–12,160, doi:10.5194/acp-10-12149-2010.

Liang, C. K., J. F. Pankow, J. R. Odum, and J. H. Seinfeld (1997), Gas/particle partitioning of semivolatile organic compounds to model inorganic, organic, and ambient smog aerosols, *Environ. Sci. Technol.*, *31*(11), 3086–3092, doi:10.1021/es9702529.

Lipsky, E. M., and A. L. Robinson (2006), Effects of dilution on fine particle mass and partitioning of semivolatile organics in diesel exhaust and wood smoke, *Environ. Sci. Technol.*, *40*(1), 155–162, doi:10.1021/Es050319p.

McMeeking, G. R., et al. (2009), Emissions of trace gases and aerosols during the open combustion of biomass in the laboratory, *J. Geophys. Res.*, *114*, D19210, doi:10.1029/2009JD011836.

Pierce, J. R., I. Riipinen, M. Kulmala, M. Ehn, T. Petaja, H. Junninen, D. R. Worsnop, and N. M. Donahue (2011), Quantification of the volatility of secondary organic compounds in ultrafine particles during nucleation events, *Atmos. Chem. Phys.*, *11*(17), 9019–9036, doi:10.5194/acp-11-9019-2011.

Ranjan, M., A. A. Presto, A. A. May, and A. L. Robinson (2012), Temperature dependence of gas-particle partitioning of primary organic aerosol emissions from a small diesel engine, *Aerosol Sci. Technol.*, *46*(1), 13–21, doi:10.1080/02786826.2011.602761.

Riipinen, I., J. R. Pierce, N. M. Donahue, and S. N. Pandis (2010), Equilibrium time scales of organic aerosol inside thermodenuders: Evaporation kinetics versus thermodynamics, *Atmos. Environ.*, *44*(5), 597–607, doi:10.1016/j.atmosenv.2009.11.022.

Robinson, A. L., N. M. Donahue, M. K. Shrivastava, E. A. Weitkamp, A. M. Sage, A. P. Grieshop, T. E. Lane, J. R. Pierce, and S. N. Pandis (2007), Rethinking organic aerosols: Semivolatile emissions and photochemical aging, *Science*, *315*(5816), 1259–1262, doi:10.1126/science.1133061.

Robinson, A. L., A. P. Grieshop, N. M. Donahue, and S. W. Hunt (2010), Updating the conceptual model for fine particle mass emissions from combustion systems, *J. Air Waste Manage. Assoc.*, *60*(10), 1204–1222, doi:10.3155/1047-3289.60.10.1204.

Rogge, W. F., L. M. Hildemann, M. A. Mazurek, G. R. Cass, and B. R. T. Simoneit (1998), Sources of fine organic aerosol. 9. Pine, oak and synthetic log combustion in residential fireplaces, *Environ. Sci. Technol.*, *32*(1), 13–22, doi:10.1021/es960930b.

Roth, C. M., K. U. Goss, and R. P. Schwarzenbach (2005), Sorption of a diverse set of organic vapors to diesel soot and road tunnel aerosols, *Environ. Sci. Technol.*, *39*(17), 6632–6637, doi:10.1021/Es049204w.

Saleh, R., A. Shihadeh, and A. Khlystov (2009), Determination of evaporation coefficients of semi-volatile organic aerosols using an integrated

volume-tandem differential mobility analysis (IV-TDMA) method, *J. Aerosol Sci.*, *40*(12), 1019–1029, doi:10.1016/j.jaerosci.2009.09.008.

Saleh, R., A. Shihadeh, and A. Khlystov (2011), On transport phenomena and equilibration time scales in thermodenuders, *Atmos. Meas. Tech.*, *4*(3), 571–581, doi:10.5194/amt-4-571-2011.

Saleh, R., A. Khlystov, and A. Shihadeh (2012), Determination of evaporation coefficients of ambient and laboratory-generated semivolatile organic aerosols from phase equilibration kinetics in a thermodenuder, *Aerosol Sci. Technol.*, *46*(1), 22–30, doi:10.1080/02786826.2011.602762.

Schauer, J. J., M. J. Kleeman, G. R. Cass, and B. R. T. Simoneit (2001), Measurement of emissions from air pollution sources. 3. C-1-C-29 organic compounds from fireplace combustion of wood, *Environ. Sci. Technol.*, *35*(9), 1716–1728, doi:10.1021/es001331e.

Seinfeld, J. H., and S. N. Pandis (2006), *Atmospheric chemistry and physics from air pollution to climate change*, p. xxviii, 1203 pp., J. Wiley, Hoboken, N. J.

Turpin, B. J., P. Saxena, and E. Andrews (2000), Measuring and simulating particulate organics in the atmosphere: problems and prospects, *Atmos. Environ.*, *34*(18), 2983–3013, doi:10.1016/S1352-2310(99)00501-4.

Watson, J. G., et al. (2011), Particulate emission factors for mobile fossil fuel and biomass combustion sources, *Sci. Total Environ.*, *409*(12), 2384–2396, doi:10.1016/j.scitotenv.2011.02.041.

Yatavelli, R. L. N., F. Lopez-Hilfiker, J. D. Wargo, J. R. Kimmel, M. J. Cubison, T. H. Bertram, J. L. Jimenez, M. Gonin, D. R. Worsnop, and J. A. Thornton (2012), A chemical ionization high-resolution time-of-flight mass spectrometer coupled to a micro orifice volatilization impactor (MOVI-HRToF-CIMS) for analysis of gas and particle-phase organic species, *Aerosol Sci. Technol.*, *46*(12), 1313–1327, doi:10.1080/02786826.2012.712236.

Zhang, Q., et al. (2007), Ubiquity and dominance of oxygenated species in organic aerosols in anthropogenically influenced Northern Hemisphere midlatitudes, *Geophys. Res. Lett.*, *34*, L13801, doi:10.1029/2007GL029979.

Author Query Form

Dear Author,

During the copyediting of your paper, the following queries arose. Please respond to these by annotating your proofs with the necessary changes/additions.
- If you intend to annotate your proof electronically, please refer to the E-annotation guidelines.
- If you intend to annotate your proof by means of hard-copy mark-up, please refer to the proof mark-up symbols guidelines. If manually writing corrections on your proof and returning it by fax, do not write too close to the edge of the paper. Please remember that illegible mark-ups may delay publication.

Whether you opt for hard-copy or electronic annotation of your proofs, we recommend that you provide additional clarification of answers to queries by entering your answers on the query sheet, in addition to the text mark-up.

Query No.	Query	Remark
Q1	AUTHOR: Please provide the initial of the author's name and also the year of publication.	
Q2	AUTHOR: Please provide the definition of "VBS".	
Q3	AUTHOR: Page number "21" of Reference "Fuentes and McFiggans" has been changed to "735–757". Please confirm that this is correct.	

USING e-ANNOTATION TOOLS FOR ELECTRONIC PROOF CORRECTION

Required software to e-Annotate PDFs: <u>Adobe Acrobat Professional</u> or <u>Adobe Reader</u> (version 7.0 or above). (Note that this document uses screenshots from <u>Adobe Reader X</u>)
The latest version of Acrobat Reader can be downloaded for free at: <u>http://get.adobe.com/uk/reader/</u>

Once you have Acrobat Reader open on your computer, click on the Comment tab at the right of the toolbar:
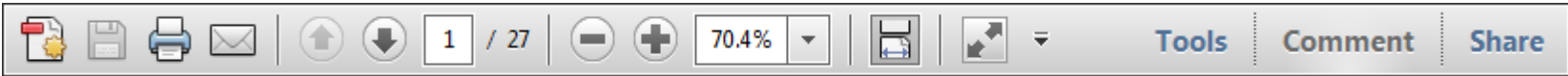
This will open up a panel down the right side of the document. The majority of tools you will use for annotating your proof will be in the Annotations section, pictured opposite. We've picked out some of these tools below:

---
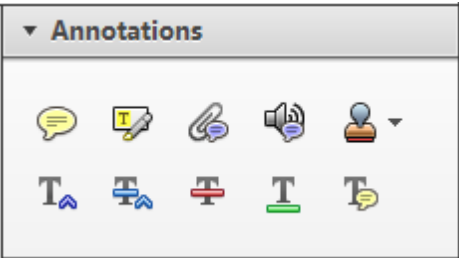
1. Replace (Ins) Tool – for replacing text.

 Strikes a line through text and opens up a text box where replacement text can be entered.

How to use it

- Highlight a word or sentence.
- Click on the Replace (Ins) icon in the Annotations section.
- Type the replacement text into the blue box that appears.

---
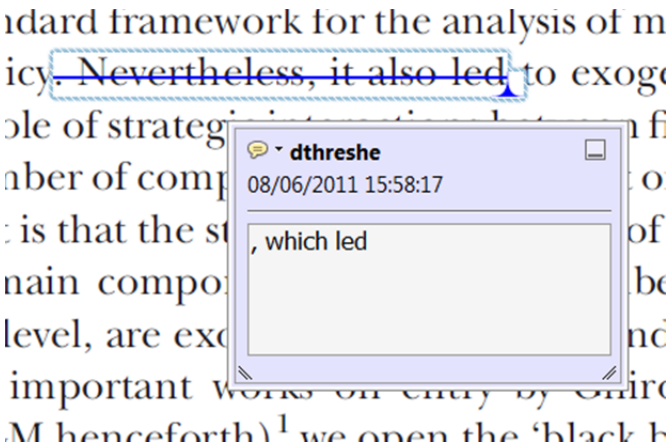
2. Strikethrough (Del) Tool – for deleting text.

 Strikes a red line through text that is to be deleted.

How to use it

- Highlight a word or sentence.
- Click on the Strikethrough (Del) icon in the Annotations section.

---
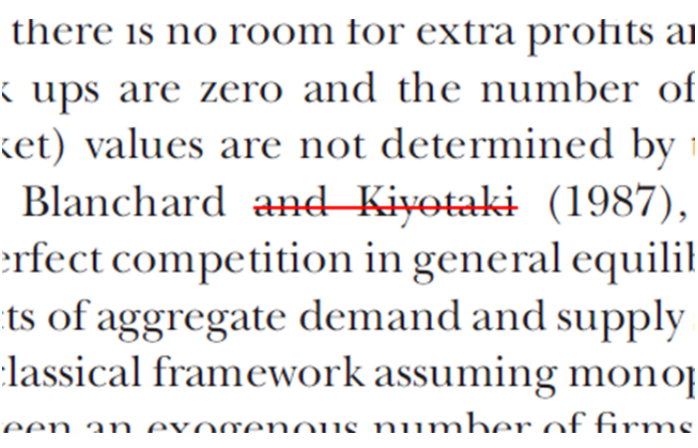
3. Add note to text Tool – for highlighting a section to be changed to bold or italic.

 Highlights text in yellow and opens up a text box where comments can be entered.

How to use it

- Highlight the relevant section of text.
- Click on the Add note to text icon in the Annotations section.
- Type instruction on what should be changed regarding the text into the yellow box that appears.

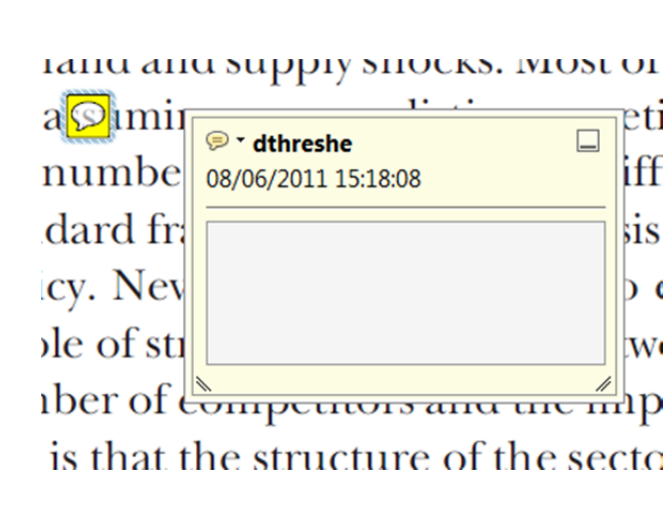---
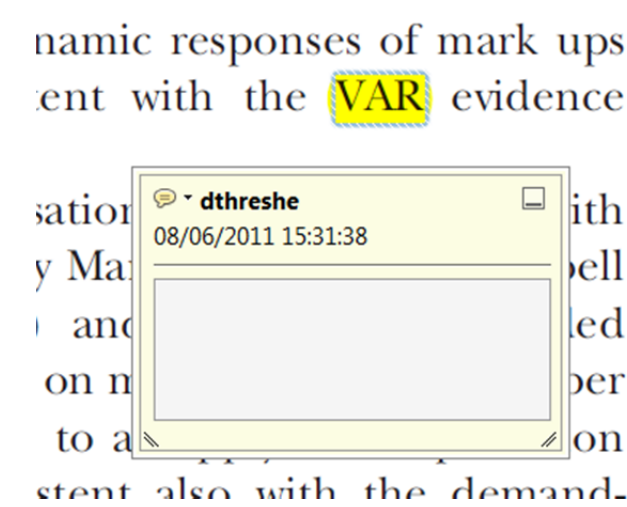
4. Add sticky note Tool – for making notes at specific points in the text.

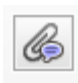 Marks a point in the proof where a comment needs to be highlighted.

How to use it

- Click on the Add sticky note icon in the Annotations section.
- Click at the point in the proof where the comment should be inserted.
- Type the comment into the yellow box that appears.

USING e-ANNOTATION TOOLS FOR ELECTRONIC PROOF CORRECTION

5. Attach File Tool – for inserting large amounts of text or replacement figures.

Inserts an icon linking to the attached file in the appropriate pace in the text.

How to use it

- Click on the Attach File icon in the Annotations section.
- Click on the proof to where you'd like the attached file to be linked.
- Select the file to be attached from your computer or network.
- Select the colour and type of icon that will appear in the proof. Click OK.

END
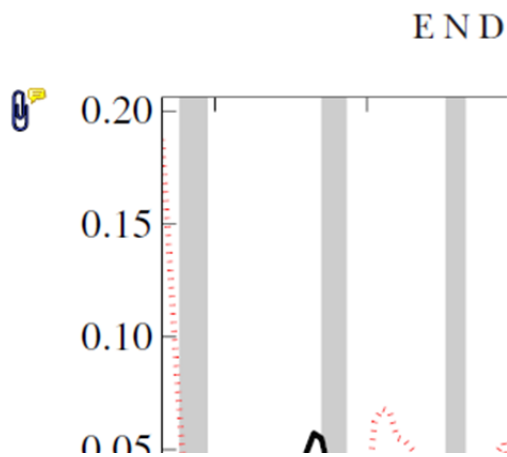
6. Add stamp Tool – for approving a proof if no corrections are required.

Inserts a selected stamp onto an appropriate place in the proof.

How to use it

- Click on the Add stamp icon in the Annotations section.
- Select the stamp you want to use. (The Approved stamp is usually available directly in the menu that appears).
- Click on the proof where you'd like the stamp to appear. (Where a proof is to be approved as it is, this would normally be on the first page).
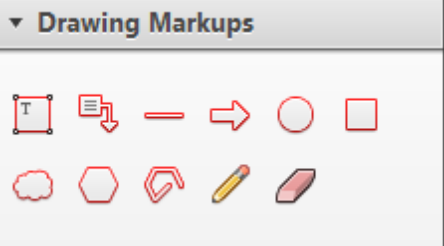

7. Drawing Markups Tools – for drawing shapes, lines and freeform annotations on proofs and commenting on these marks.

Allows shapes, lines and freeform annotations to be drawn on proofs and for comment to be made on these marks..

How to use it

- Click on one of the shapes in the Drawing Markups section.
- Click on the proof at the relevant point and draw the selected shape with the cursor.
- To add a comment to the drawn shape, move the cursor over the shape until an arrowhead appears.
- Double click on the shape and type any text in the red box that appears.
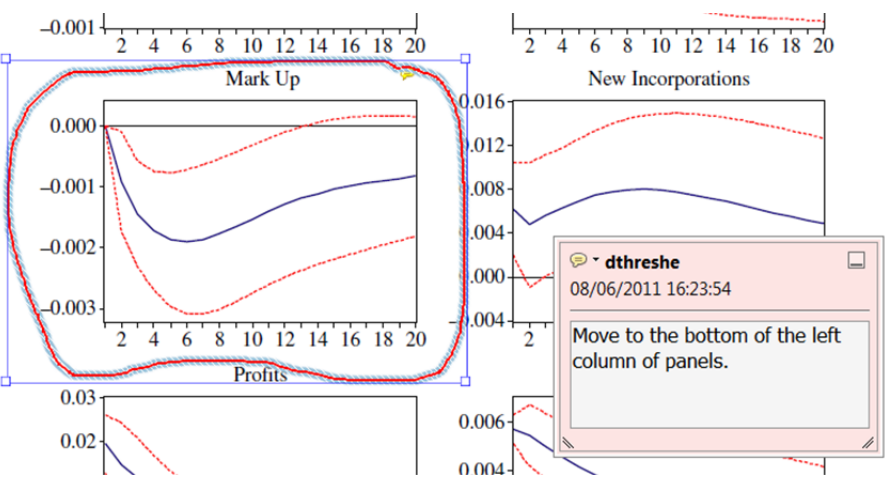
For further information on how to annotate proofs, click on the **Help** menu to reveal a list of further options:

WILEY-BLACKWELL
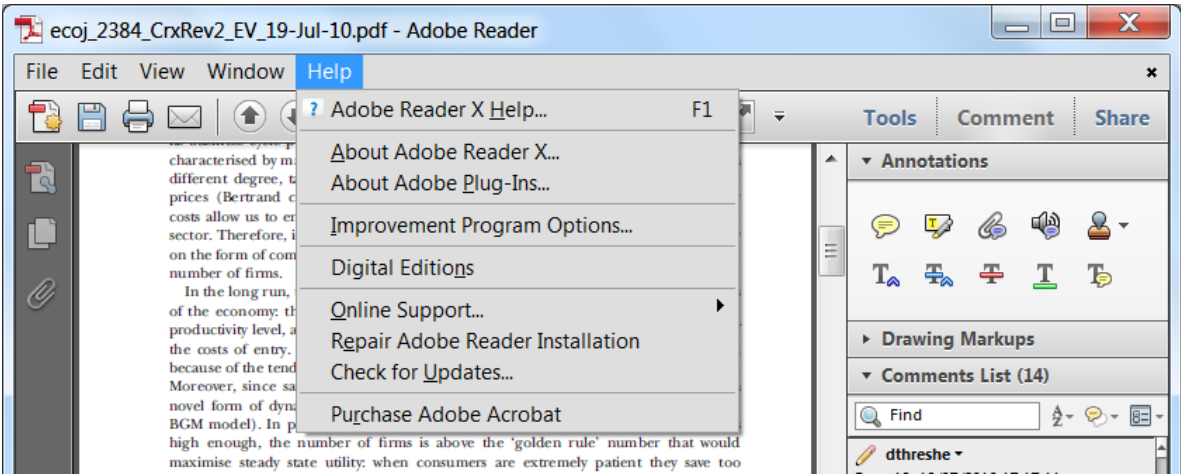
Additional reprint and journal issue purchases

Should you wish to purchase additional copies of your article,
 please click on the link and follow the instructions provided:
 https://caesar.sheridan.com/reprints/redir.php?pub=10089&acro=JGRD

Corresponding authors are invited to inform their co-authors of
the reprint options available.

Please note that regardless of the form in which they are acquired,
reprints should not be resold, nor further disseminated in electronic form, nor
deployed in part or in whole in any marketing, promotional or educational
contexts without authorization from Wiley. Permissions requests should be
directed to mailto: permissionsus@wiley.com

For information about 'Pay-Per-View and Article Select' click on the following
link: http://wileyonlinelibrary.com/ppv